

# C 1 Interfacial Pattern Formation

K. Kassner

Institut für Theoretische Physik /

Computerorientierte Theoretische Physik

Otto-von-Guericke-Universität Magdeburg

## Contents

<b>1</b>	<b>Introduction</b>	<b>2</b>
<b>2</b>	<b>Interfacial instabilities</b>	<b>4</b>
2.1	Mullins-Sekerka instability . . . . .	5
2.2	Saffman-Taylor instability . . . . .	6
<b>3</b>	<b>Mathematical models</b>	<b>7</b>
3.1	Continuum model for solidification . . . . .	7
3.2	Modeling viscous fingering . . . . .	10
<b>4</b>	<b>Stability of stationary solutions</b>	<b>11</b>
4.1	Planar interface . . . . .	12
4.2	Linear stability analysis of the planar solidification front . . . . .	12
4.3	Weakly nonlinear analysis . . . . .	15
<b>5</b>	<b>Nonlinear dynamics – dendrites and fingers</b>	<b>16</b>
5.1	Ivantsov solution . . . . .	16
5.2	Selection theory . . . . .	17
<b>6</b>	<b>Doublons and more complex patterns</b>	<b>19</b>
<b>7</b>	<b>Summary and outlook</b>	<b>22</b>

# 1 Introduction

With a school on computational aspects of condensed matter physics, it is appropriate to put the emphasis on methodology. However, not all presentations may predominantly cover numerical or algorithmic approaches, because in some cases it is necessary to first introduce physical concepts that not everybody might be familiar with. This is such a contribution.

The main questions in the field of pattern formation can be phrased in a relatively simple manner. Why do patterns arise spontaneously from a homogeneous environment (or at least an environment less structured than the pattern)? How do they organize themselves? In particular, how is one alternative chosen out of several, often many, possible ones? Since we are physicists, we are interested in measurable, quantitative aspects of conspicuous features of the pattern under scrutiny. We may then ask, how the length scale of a pattern is selected – or its velocity, if it is moving.

First, we ought to have some general idea what kind of patterns we are talking about. Clearly, the atoms of a crystal form a nice and regular pattern at the microscopic scale. This kind of structure occurs in thermodynamic equilibrium because the ordered state minimizes the free energy of the system, reflecting a compromise between energetic and entropic forces. These microscopic patterns are well understood, we have good intuition about them, and they are *not* the subject to be discussed here.

Rather, the focus shall be on patterns that arise in a somewhat counterintuitive manner, appearing to defy the second law of thermodynamics by producing order in a less ordered environment, and doing so spontaneously, *i.e.*, without the intervention of a planning entity. Since the second law is not really violated, entropy must be exported by the pattern, which means it has to be kept far from equilibrium by some driving mechanism. We have thus identified one important ingredient for macroscopic pattern formation, a *nonequilibrium* situation leading to dissipation.<sup>1</sup> A second important ingredient is *nonlinearity* of the governing equations. Macroscopic systems are usually described in terms of continuous variables. The dynamical description of an extended system requires at least the time and one variable for spatial extension, meaning that the basic equations are partial differential equations. Now consider a simple linear partial differential equation, such as the wave equation:

$$\frac{\partial^2 u}{\partial t^2} - c^2 \frac{\partial^2 u}{\partial x^2} = 0, \quad (1)$$

where  $u$  is the amplitude of some excitation and  $c$  the speed of the waves. A plane wave ansatz

$$u = u_k \exp\{i(kx - \omega t)\} \quad (2)$$

solves this equation, provided the dispersion relation

$$\omega^2 = c^2 k^2 \quad (3)$$

is satisfied. That is, we can find solutions at arbitrary wavelength  $2\pi/k$ . The superposition principle guarantees that any sum of these solutions is a solution again, which is the reason why the general solution to (1) may be obtained by expanding the field  $u$  in a Fourier series. But this means that no particular wavelength can be preferred by the equation.<sup>2</sup> Since having one

<sup>1</sup>There are exceptions to this rule. Ferrofluids form macroscopic equilibrium structures in magnetic fields. Solitons are dynamical structures not driven by dissipation.

<sup>2</sup>Such a preference could of course be brought about by boundary conditions. We would however not regard patterns as self-organized, if they are determined this way by the geometry of the system – Chladni's sound figures may serve as a case in point.

or several preferred length scales is the signature of a pattern, we cannot expect self-organized structures to be describable by equations satisfying the superposition principle. Hence, models for pattern forming systems have to be nonlinear (systems of) equations.

Nature abounds with phenomena of self-organization resulting from nonlinear dynamics. While this may be visible most strikingly in biology, many examples can be pointed out from other disciplines such as physics, chemistry, meteorology, ecology, cosmology, to name but a few. Physical systems have the advantage that often their basic nonlinear equations are well known, so a detailed theoretical investigation may start from a sound modeling basis, whereas experiments may focus on precise quantitative questions. A number of paradigmatic setups have been devised to bring out the characteristic phenomena. The best-studied of these are hydrodynamic systems, for example the Rayleigh-Bénard and the Taylor-Couette experiments, electrohydrodynamic convection or else parametrically excited surface waves. Aspects of hydrodynamic systems are discussed in the lecture by W. Zimmermann.

Furthermore, self-organization and pattern formation are found, besides many more or less obvious examples from biology (such as the patterns in coats of animals such as zebras and leopards), in chemical reaction diffusion systems, with structures ranging from spiral waves [1] to Turing patterns [2, 3], in convective flame fronts [4], producing cellular patterns, in nonlinear optics [5], in electrical discharges within plasmas and semiconductors [6, 7], and in solidification and viscous fingering. The last two phenomena will be discussed in more detail in the following. They share the characteristic feature that their dynamics is essentially affected by the presence of an *interface*, either between a solid and a fluid or between two immiscible fluids. How problems involving complex interfaces are treated numerically using the phase-field method is explained in the lecture by B. Nestler presenting, in particular, applications to solidification.

In the continuing effort to understand these phenomena, a few general ideas have been developed. The analogy, on a mean-field level, between phase transitions and nonequilibrium transitions from one ordered pattern (including the homogeneous structureless state) to another was apparently first pointed out in laser physics [8]. As with phase transitions, one can often identify a symmetry that is broken during the transformation of the structure. Of course, nonequilibrium systems show a much larger variety of behaviours than equilibrium systems. Nonequilibrium transitions are intimately connected with *instabilities* that destroy one structure to clear the way for a new one. Close to the threshold, where a mode becomes unstable, its growth is very slow. This leads to a separation of time scales allowing adiabatic elimination of fast variables, enabling a description in terms of few relevant variables serving as order parameters. Sometimes this reduction to *amplitude equations* is restricted to such a small regime about the critical point that it is next to useless for practical purposes. Then one has to have recourse to semianalytical (phase equation) or numerical approaches [9].

The concepts developed in the physical description of dynamics far from equilibrium have found applications in other sciences. On the other hand, physics has taken over some of the vocabulary of these disciplines. Most notable is the use of Darwin's notions [10] of *competition* and *selection* in the discussion of nonequilibrium systems. In a laser, all possible modes compete for the pumping power but only a few (or just one) are ordinarily selected, *i.e.*, they stay "alive", feeding themselves from the power input. In solidification, different possible modes of structural organization may compete for the incoming flux of material. If one of them grows faster than its competitors, it will be selected, because it will simply outgrow them. More subtle selection problems are, *e.g.*, the question of the selection of length scales and of the growth velocity for given morphologies.

Since there is such a huge variety of pattern-forming systems, an introductory lecture cannot treat all of them. I will therefore focus on pattern formation via motion of an interface, mostly because solidification systems are those I know best, but also because they provide an extremely good motivation for the phase-field method, which is one of the most versatile numerical approaches to interface dynamics.

## 2 Interfacial instabilities

If you ask a random person to describe solidification of a crystal, most probably the growth of a simple regular shape consisting of highly symmetric polyhedra will be depicted. A salt (NaCl) crystal, when grown from solution, essentially is a cube, sometimes consists of several ones. Now consider a snowflake, normally a single crystal, too. Figure 1 displays a hand-drawn example. Evidently, this object does display the regularity of the underlying crystal structure as well, but nonetheless there is a profound difference when comparing with the simple shape of a salt crystal.

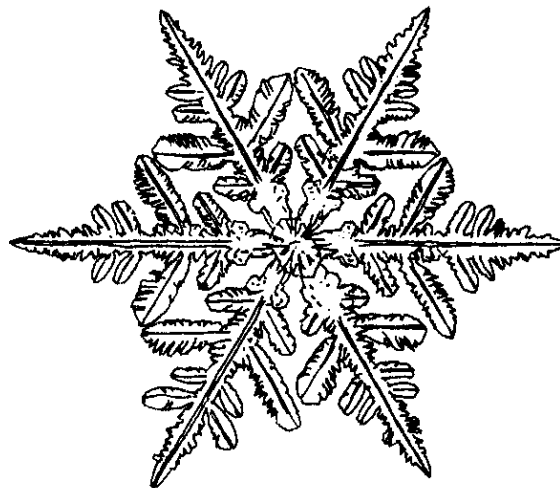


**Fig. 1:** Drawing of a snowflake, after a photograph by Furukawa [11].

The snowflake has a property that a salt cube has not – complexity. One realizes this when trying to give an accurate verbal description of a shape such as the one displayed in Fig. 1. Its six main arms have a characteristic structure, resembling that of a tree, hence the name *dendrites* for these crystals.<sup>3</sup> The symmetry is only approximate, not exact, and it does not entirely determine the shape. In fact, it is proverbial knowledge that no two snowflakes are alike. Apparently, it is this interplay between symmetry and complexity that makes us feel snowflakes are esthetically pleasing objects.

Scientific interest in dendritic growth is not only driven by the fundamental considerations outlined above, but also by its technological relevance. The microstructure of most cast alloys is dendritic, and it is essentially the size of the dendritic patterns that determines material properties such as strength and ductility. Minor improvements in the control of the microstructure can result in major reductions of production costs.

<sup>3</sup>After the Greek  $\tau\acute{o}$   $\delta\acute{\epsilon}\nu\delta\rho\omicron\nu$ , meaning *the tree*.

## 2.1 Mullins-Sekerka instability

Snowflakes grow in an environment of undercooled vapour. It is relatively easy to understand why this must lead to a complex shape, if we assume the growth to be controlled mostly by the transport of latent heat. During solidification, the latent heat produced must be transported away from the surface of the solid and through the vapour – otherwise the solid would heat up until growth stops. Then simple shapes become unstable. Roughly speaking, this is because the crystal can get rid of heat more efficiently having a large surface than having a small one. Simple shapes have smaller surfaces than complex ones of the same volume.

Figure 2 depicts, in the left panel, a solid exhibiting a planar interface in contact with its undercooled vapour (or melt). The dashed lines represent the isotherms in the fluid phase. Assume then that there is a fluctuation of the interface shape leading to a protrusion of the solid into the fluid. Ahead of point  $A$ , the isotherms will be compressed a little which leads to an increase in the magnitude of the temperature gradient. Since the heat current  $j$  is proportional to the temperature gradient ( $j = -\chi_{\text{th}} \nabla T$ , with thermal conductivity  $\chi_{\text{th}}$ ) this means that latent heat is more rapidly transported into the fluid from point  $A$  than from point  $B$ . Therefore, crystallization will accelerate at  $A$ , the perturbation grows, we have an instability.

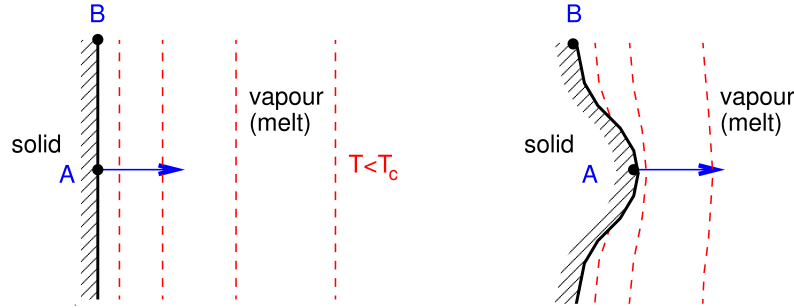


**Fig. 2:** Illustration of the Mullins-Sekerka instability.

This instability, named after Mullins and Sekerka who were the first to give its quantitative description [12], would eventually lead to a complete break-up of the structure into ever finer parts, were it not for stabilizing counter effects.

Surface tension provides such an effect, because it influences the melting temperature of the solid. In thermal equilibrium, the temperature of the interface is

$$T(\kappa) = T_m \left( 1 - \frac{\gamma \kappa}{L} \right), \quad (4)$$

where  $T_m$  is the bulk melting temperature,  $\gamma$  the surface tension, here assumed isotropic,  $L$  the latent heat per unit volume, and  $\kappa$  the curvature of the interface in a two-dimensional (2D) system and the sum of the two principal curvatures in a 3D one.  $\kappa$  is counted positive for a locally convex solid.

This so-called *Gibbs-Thomson relation* has been taken into account in drawing Fig. 2. In the right panel of the figure, the temperature at  $A$  (where  $\kappa > 0$ ) is below that at  $B$  (where  $\kappa < 0$ ). The interface no longer is an isotherm but is cut by isotherms. In fact, if the isotherms were not allowed to cross the interface, the (absolute value of the) temperature gradient would have to be larger than it is in reality. This demonstrates, that surface tension, leading to a smaller temperature gradient, acts stabilizing indeed.

## 2.2 Saffman-Taylor instability

In viscous fingering experiments, an inviscid fluid displaces a viscous one. All the action takes place between two closely spaced plates. A setup that leads to spectacular patterns consists of circular plates with the inviscid fluid, usually air, injected at the center. Figure 3 shows an experimental example.

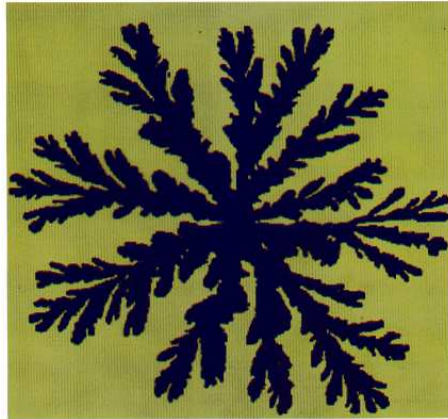


**Fig. 3:** *Viscous fingering in a circular geometry. The illumination was chosen such that the less viscous fluid appears dark, whereas the other one makes up the bright background.*

In a long rectangular so-called Hele-Shaw cell, patterns become less spectacular but are more readily analysed. With ordinary (*i.e.*, Newtonian) fluids, a single finger emerges approaching a definite width that is usually close to one half of the cell width, compare Fig. 4.

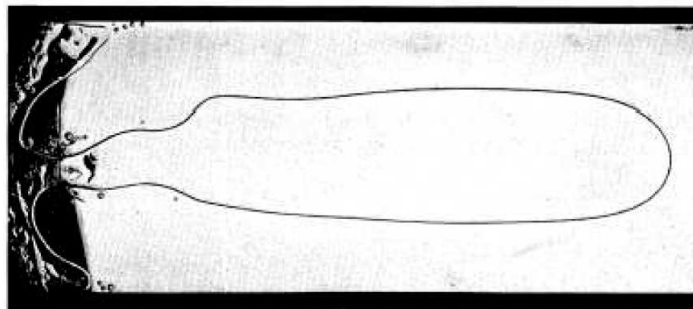


**Fig. 4:** *Saffmann-Taylor finger, from the original work [13].*

In order to understand the origin of the complexity of a pattern such as the one in Fig. 3, let us consider an originally planar interface between the two fluids in a rectangular geometry (Fig. 5). The displacing fluid to the left has very low viscosity with the consequence that its pressure is essentially constant. In the displaced fluid on the right, the pressure decreases towards its far-field value; the dashed lines are isobars. It is then important to know that in the narrow gap between the two plates the fluids move like liquids in a porous medium. This motion is described by Darcy's law stating simply that the velocity is proportional to the negative pressure gradient.

But then we can make an argument that corresponds exactly to the one given for crystal growth above, with the role of the heat current replaced by that of the pressure gradient. A small

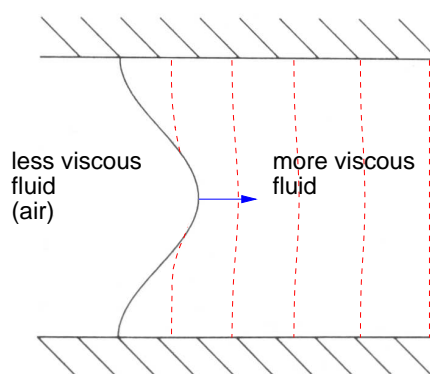


**Fig. 5:** *Origin of the Saffman-Taylor instability.*

protrusion of the interface will lead to an increase in the pressure gradient and hence have a tendency to grow faster, driven by the additional gradient. Surface tension is stabilizing again: instead of the Gibbs-Thomson relation we have the capillary overpressure, decreasing the pressure and with it the pressure gradient ahead of a convexely curved interface. The system bears strong similarities with the crystal growth situation and it is in fact easy to visualize Fig. 3 as a snowflake from which crystalline anisotropy has been removed.

### 3 Mathematical models

#### 3.1 Continuum model for solidification

For simplicity, we consider a pure substance growing into its undercooled melt, assume that the thermal diffusion constant is the same in both phases (*symmetric model*), restrict ourselves to two spatial dimensions and neglect convective flows in the fluid phase. The first assumption merely serves to fix the language – we will view temperature as the diffusing quantity. The same model is also valid for chemical diffusion in two-component alloys [14], albeit the assumption of similar diffusion coefficients in both phases would then not be realistic.<sup>4</sup> Thermal diffusivities in solids and their melts, on the other hand, are normally of the same order of magnitude, differing usually by a factor of two or so.<sup>5</sup> In neglecting convection, we intend by no means to imply that convection is unimportant in practice – in fact it does play a crucial role in the casting of alloys. However, it is not necessary for the creation of dendritic patterns. Therefore, when attempting to understand this process, it is legitimate to leave flows out of the model in a first approach. Moreover, experimentalists have managed to eliminate convection almost completely in setups using model substances such as the plastic crystal succinonitrile [15, 16], thus obtaining dendritic structures that should correspond to the theoretical description. This situation usually is referred to as *diffusion-limited growth*.

Transport in the bulk is then described by the diffusion equation for the temperature field, which

<sup>4</sup>In that case, the *one-sided model* is more useful, in which chemical diffusion in the solid is neglected. Then only the liquid domain needs to be described in detail.

<sup>5</sup>The assumption of equal thermal diffusivities would be a bad approximation for a solid in contact with its vapour. This is one of several reasons, why we will not try to model snowflakes directly but rather consider a solid-liquid system.

we normalize as:  $u(\mathbf{x}, t) = [T(\mathbf{x}, t) - T_\infty] / (L c_p^{-1})$ . This is the deviation of the local nondimensional temperature at point  $\mathbf{x}$  from the imposed temperature at infinity,  $T_\infty$ ;  $c_p$  is the heat capacity per unit volume. Explicitly,

$$\frac{\partial u}{\partial t} = D \nabla^2 u, \quad (5)$$

with thermal diffusivity  $D$ .

Local heat conservation at the *interface* implies  $L v_n = -c_p D (\partial T / \partial n|_\ell - \partial T / \partial n|_s)$ , where  $v_n$  is the normal velocity of the advancing interface and the subscripts  $\ell, s$  denote the liquid and solid sides of the advancing interface, respectively. This continuity equation is often called *Stefan condition*. Its left-hand side describes the latent heat generated per time unit by the growth of the solid, the right-hand side is the difference of heat fluxes into the liquid and out of the solid. Rewritten in terms of the normalized temperature field, this becomes

$$v_n = -D \left( \frac{\partial u}{\partial n} \Big|_\ell - \frac{\partial u}{\partial n} \Big|_s \right). \quad (6)$$

Furthermore, we have a boundary condition from the Gibbs-Thomson relation which reads

$$u|_\ell = u|_s = \Delta - d\kappa. \quad (7)$$

Herein,  $\Delta$  is the nondimensional undercooling  $\Delta = (T_m - T_\infty) / (L c_p^{-1})$  and  $d$  is the so-called capillary length, given by

$$d = [\gamma(\vartheta) + \gamma''(\vartheta)] \frac{T_m}{L^2 / c_p}. \quad (8)$$

The curvature  $\kappa$  at an interface point  $\mathbf{x} = (x, \zeta(x, t))$  may be calculated according to  $\kappa(\mathbf{x}, t) = -\zeta_{xx}(x, t) / (1 + \zeta_x(x, t)^2)^{3/2}$ . Equation (7) is a generalization, in 2D, of eq. (4) to the case of anisotropic surface tension [17].  $\vartheta$  is the angle between the interface normal and a fixed direction.

To complete the description, we need boundary conditions at infinity. We simply require, for  $|\mathbf{x}| \rightarrow \infty$ ,

$$u(\mathbf{x}, t) \rightarrow \begin{cases} 0 & \text{in the liquid} \\ \Delta & \text{in the solid} \end{cases}. \quad (9)$$

Note that  $d$  is the only quantity with the dimension of a length that enters our equations. Therefore,  $d$  must determine the length scale of any pattern forming under the dynamics described.

At this point, some readers might complain. What is written here seems to just be a linear equation of motion [Eq. (5)] plus boundary conditions [Eqs. (6) through (9)], while the introduction emphasized that nonlinearity is necessary for pattern formation. But appearances are deceiving. A system of equations is linear only if the equation for each of its variables is linear. In fact, the problem to be solved comprises *two* variables, namely the diffusion field and the position of the interface. The equation of motion determining the latter is Eq. (6). If we denote the interface position by  $\mathbf{x}_i$ , then  $v_n = \mathbf{n} \cdot d\mathbf{x}_i / dt$ . This is an equation only for the normal component of the interface velocity, but more is not needed – the tangential component is indeterminate. Moving interface points around along the interface, that is tangentially, obviously does not change the interface itself.<sup>6</sup> We shall see below that the equation for the interface position is strongly nonlinear, rendering the total problem nonlinear.

<sup>6</sup>A definite tangential velocity may be ascribed only to the endpoints of an interface – if there are any.



If we take into account that we have to solve for two quantities, the temperature field in the two-dimensional bulk and the interface position in terms of a local displacement variable, defined on a curve, then equation counting comes out just right. We have one equation of motion for each of these two fields, these are Eqs. (5) and (6), and we have a boundary condition for the diffusion field on each of the external and internal boundaries of the system, these are Eqs. (7) and (9). If the interface position were *prescribed*, then Eq. (6) would constitute a second boundary condition for the diffusion equation, which is one too many, rendering the problem overdetermined. But the boundary is free to move, and eq. (6) is just what we need to calculate its motion, once the diffusion equation has been solved in the two domains. This kind of task is called a *moving boundary problem* and belongs to the mathematically notoriously difficult problems.

Nevertheless, the fact that the bulk equations of motion of the model are linear is beneficial. It allows us to recast them into the form of boundary integral expressions by use of Green's functions. One can then derive a closed integral equation for the interface position. Such a representation is very useful both in numerical and analytic work.

It is advantageous to consider diffusion in a frame of reference moving at constant velocity  $V$ . Defining the direction of motion to be the  $z$  direction, we have

$$\hat{L}_{\mathbf{x},t} u(\mathbf{x}, t) \equiv \left( -\frac{\partial}{\partial t} + D\nabla^2 + V \frac{\partial}{\partial z} \right) u(\mathbf{x}, t) = 0. \quad (10)$$

A *Green's function* of the differential operator  $\hat{L}_{\mathbf{x},t}$  is a function  $G(\mathbf{x}, t; \mathbf{x}', t')$  satisfying the inhomogeneous equation  $\hat{L}_{\mathbf{x},t} G(\mathbf{x}, t; \mathbf{x}', t') = -\delta(\mathbf{x} - \mathbf{x}')\delta(t - t')$  and the adjoint equation

$$\hat{L}_{\mathbf{x}',t'}^+ G(\mathbf{x}, t; \mathbf{x}', t') = \left( \frac{\partial}{\partial t'} + D\nabla'^2 - V \frac{\partial}{\partial z'} \right) G(\mathbf{x}, t; \mathbf{x}', t') = -\delta(\mathbf{x} - \mathbf{x}')\delta(t - t'). \quad (11)$$

Note first that  $\hat{L}$  is not self-adjoint. The two equations are different. This is one reason for the mathematical difficulty of the problem – there are no variational techniques available to produce a simpler formulation. Second, these equations determine  $G(\mathbf{x}, t; \mathbf{x}', t')$  only up to a solution of the corresponding homogeneous equation, and we can use *any* Green's function of our operator. This makes life easier, since it is not too difficult to find a particular Green's function not required to satisfy complicated boundary conditions. In our case, an appropriate function is given by

$$G(\mathbf{x}, t; \mathbf{x}', t') = \frac{\Theta(t - t')}{4\pi D(t - t')^{d_e/2}} \exp \left\{ -\frac{[\mathbf{x} - \mathbf{x}' - \mathbf{v}(t - t')]^2}{4D(t - t')} \right\}, \quad (12)$$

where the Heaviside function  $\Theta(t - t')$  ensures causality,  $\mathbf{v} = V\mathbf{e}_z$ , and  $d_e$  is the (Euclidean) dimension of space (*i.e.*,  $d_e = 2$  or  $d_e = 3$ ). To obtain integral equations, one multiplies eq. (10) (rewritten in primed coordinates) by  $G(\mathbf{x}, t; \mathbf{x}', t')$ , eq. (11) by  $u(\mathbf{x}', t')$ , integrates over the liquid and solid domains, respectively, and utilizes Green's theorem to reduce expressions to boundary integrals. For an explicit description see Refs. [18, 19]. Here we skip all details and just give the final result for the symmetric model

$$u(\mathbf{x}, t) = \Delta - d(\vartheta)\kappa = \int_{-\infty}^t dt' \int_{\Gamma_{sl}} d\Gamma' \left[ V + \frac{\partial}{\partial t'} \zeta(\mathbf{x}', t') \right] n'_z G(\mathbf{x}, t; \mathbf{x}', t'), \quad (13)$$

where  $\Gamma_{sl}$  is the integration contour (along the interface) and  $n'_z$  the  $z$  component of the normal vector on it. This equation has a very simple interpretation: because the diffusivity is the same in both phases here, the moving interface affects the diffusion field only by acting as a source of latent heat. On account of eq. (6), the strength of this source is just  $v_n(\mathbf{x}', t') = (V + \partial_{t'}\zeta)n'_z$ . The total field is then simply obtained through integration of the source strength multiplied by the propagator  $G(\mathbf{x}, t; \mathbf{x}', t')$  on the entire interface.

Equation (13) is an integrodifferential equation for the interface position alone. The field  $u$  has been eliminated by expressing it and its normal derivative on the boundary with the help of the Gibbs-Thomson and the Stefan conditions. The integral equation is quite obviously nonlinear, since the quantity  $\zeta(\mathbf{x}, t)$ , for which it is to be solved occurs in the argument of the Green's function. Moreover, even the curvature term on the left-hand side is nonlinear in  $\zeta$ . The equation is also *nonlocal* both in time and space, because the integrand contains the time argument  $t' \leq t$  and spatial arguments from anywhere in the domain considered.

Often, it is appropriate to assume the *quasistationary approximation* to hold, meaning that in the frame moving at the average velocity of the interface  $\partial_t\zeta(\mathbf{x}, t)$  is a slowly varying quantity. This is true for small undercoolings, when interface shape changes are much slower than diffusion in the bulk. One may then replace  $\partial_{t'}\zeta(\mathbf{x}, t')$  in the integrand by  $\partial_t\zeta(\mathbf{x}, t)$ , interchange the time and space integrations in Eq. (13) and carry out the time integral of the Green's function, which gives

$$\int_{-\infty}^t dt' G(\mathbf{x}, t; \mathbf{x}', t') = \frac{2}{(4\pi D)^{d_e/2}} e^{-\frac{\mathbf{v}(\mathbf{x}-\mathbf{x}')}{2D}} \left( \frac{|\mathbf{x}-\mathbf{x}'|}{|\mathbf{v}|} \right)^{2-d_e} K_{1-d_e/2} \left( \frac{|\mathbf{v}|}{2D} |\mathbf{x}-\mathbf{x}'| \right), \quad (14)$$

with  $K_{1-d_e/2}$  denoting the modified Bessel function of order  $1 - d_e/2$  [20]. In two dimensions, this is Macdonald's function  $K_0$ .

When this is inserted in Eq. (13), we have an equation for the interface position containing only quantities defined on the interface, at a single time. Hence, the integral equation is given on a one-dimensional domain (the interface), whereas the original partial differential equation with boundary conditions on a moving boundary was defined on a two-dimensional domain. Numerically, this reduction of dimensionality normally means a reduction of computational costs. A strategy to solve for the interface position consists in a discretisation of the integral and propagation of the interface in time according to the value of  $\partial_t\zeta(\mathbf{x}, t)$  obtained after inversion of the matrix corresponding to the steady-state Green's function. The set of techniques enabling the reduction of an  $n$ -dimensional linear partial differential equation to a problem on the  $(n-1)$ -dimensional domain boundary run under the name of *boundary integral methods*, their numerical exploitation leads to *boundary element methods*, and it was with this approach that the first quantitative simulations of two-dimensional dendritic growth [14] were performed.

### 3.2 Modeling viscous fingering

In the Saffman-Taylor problem, we consider a cell of small thickness  $b$ . As a consequence, the Reynolds number of the arising flow,  $\text{Re} = \rho U b / \mu$ , where  $\rho$  is the density,  $U$  the flow speed, and  $\mu$  the dynamic viscosity, will be small for both fluids. Then the appropriate equation of motion relating pressure  $p$  and flow velocity  $\mathbf{U}$  is the Stokes equation

$$\nabla p = \mu \nabla^2 \mathbf{U}. \quad (15)$$

It follows that if one of the two fluids has negligible viscosity, its pressure will remain constant in space. In this case of “infinite viscosity contrast”, we may restrict the model to the domain occupied by the fluid with the larger viscosity, a situation that is akin to the one-sided model of solidification discussed above.

Averaging the velocity profile over the thickness of the cell (assuming Poiseuille flow), one can show that the resulting two-dimensional profile satisfies Darcy’s law

$$\bar{\mathbf{U}} = -\frac{b^2}{12\mu} \nabla p. \quad (16)$$

From now on, we will omit the bar indicating the average along the third dimension and consider only two-dimensional velocities. Using the incompressibility condition  $\nabla \cdot \mathbf{U} = 0$ , we obtain from Eq. (16) that the pressure satisfies the Laplace equation

$$\nabla^2 p = 0. \quad (17)$$

At the interface between the two fluids, we have a kinematic condition requiring impenetrability (as well as the absence of holes) which means that the interface normal velocity must be equal to the normal velocity of the fluids. Together with Darcy’s law this gives

$$v_n = -\frac{b^2}{12\mu} \nabla p \cdot \mathbf{n} = -\frac{b^2}{12\mu} \frac{\partial p}{\partial n}, \quad (18)$$

the analogue of the Stefan condition.

Finally, we have Laplace’s law for the overpressure at a curved interface between two liquids

$$p = p_0 - \gamma \kappa, \quad (19)$$

where  $p_0$  is the constant pressure of the driving fluid (*e.g.* air) and  $\gamma$  the interface tension, which is orientation independent for a pair of ordinary fluids.<sup>7</sup>

Comparing Eqs. (17) to (19) with Eqs. (5) through (9), we note strong similarities. If we consider the one-sided model of crystal growth, obtained from the discussed equations by dropping all the terms referring to the solid, we note, in the isotropic limit, complete agreement with the boundary equations of the Saffman-Taylor problem. The remaining difference then is that we have the diffusion equation in crystal growth and the Laplace equation in viscous fingering. This also implies the necessity to modify the boundary condition for the field quantity (the pressure) at infinity, which therefore has not been written out here. After performing the quasistationary approximation in the moving frame, which is equivalent to dropping the time derivative in Eq. (10), the similarity of the two systems can be put more precisely. The Saffman-Taylor problem corresponds to the limit of vanishing average velocity  $V$  of the (isotropic variant of) the crystal growth problem, if the latter is restricted to a channel geometry.

## 4 Stability of stationary solutions

From now on, we will focus on the crystal growth problem. Results for viscous fingering will be mentioned in passing but their explicit derivation is beyond the scope of this article.

<sup>7</sup>When the experiment is done with liquid crystals, there is orientation dependence just as in the crystal growth case. In that situation, viscous fingering patterns can display dendritic morphologies.

## 4.1 Planar interface

The simplest solution of our model equations one can think of is a plane moving at constant velocity, together with an appropriate spatial profile of the diffusion field. In the moving frame, this is a *stationary* solution. Heat conservation implies that such a solution is possible only if the undercooling  $\Delta = 1$ . It takes the form

$$\begin{aligned}\zeta(x) &\equiv 0, \\ u_0(z) &= \begin{cases} e^{-Vz/D} & \text{if } z \geq 0 \text{ (liquid)} \\ 1 & \text{if } z < 0 \text{ (solid)} \end{cases}.\end{aligned}\quad (20)$$

For  $\Delta < 1$ , the behaviour of a solution that is required to be planar obtains from a so-called *similarity solution* of the model equations [21]. Such a solution often describes generic asymptotic behaviour, regardless of the initial conditions. Assuming that the diffusion field depends only on a certain combination of its arguments,  $u(x, z, t) = U(z/z_0(t)) \equiv U(w)$ , we have

$$U''(w) + \frac{z_0 \dot{z}_0}{D} w U'(w) = 0. \quad (21)$$

For this to be an equation in the variable  $w$  alone, we must have  $z_0 \dot{z}_0 = \text{const.}$  or

$$\frac{z_0 \dot{z}_0}{D} \equiv 2P \implies z_0(t) \propto (4DPt)^{1/2} \quad (22)$$

and  $U(w) \propto \int_w^\infty dw' \exp(-Pw'^2)$ . The interface sits at  $z = z_0$ , *i.e.*,  $w = 1$ , where we have to impose  $U(w) = \Delta$  which together with the continuity equation leads to

$$\Delta = \sqrt{\pi P} e^P \text{erfc}(\sqrt{P}). \quad (23)$$

Herein,  $\text{erfc}(x)$  is the complementary error function [20]. Physically, this solution describes an interface that slows down (we have  $\dot{z}_0 \sim t^{-1/2}$ ), because an increasing layer of warm liquid builds up in front of the solid. Not all the latent heat liberated is consumed by heating up the undercooled liquid to the melting temperature, at which it solidifies. The excess heat produces the ever-growing layer of warm liquid. Only when  $\Delta = 1$  is the undercooling large enough to remove all the latent heat generated and can the interface move at constant velocity. Again there is a layer of warm liquid ahead of the interface [see Eq. (20)], but its thickness remains constant.

A decelerating interface will normally not be seen in experiment if there exists another structure that can grow at constant velocity, because the latter will eventually be faster – it will outgrow the slower morphology, provided it can be “nucleated” at some time by a small perturbation.

## 4.2 Linear stability analysis of the planar solidification front

The planar front solution (20) does not set any length scale. This is natural, because the only term containing a length scale, the product  $d\kappa$ , drops from the equations for a planar front. To be sure, it is possible to *define* a length from (20), this is the so-called *diffusion length*  $\ell = 2D/V$ . However, there is nothing that determines  $V$ . The planar front can move at any velocity. Moreover, the discussion of Sec. 2 suggests that simple interface shapes will not be stable ordinarily. One way to get a first idea about typical sizes to be expected of possibly developing patterns is to do a linear stability analysis.

We start by considering a sufficiently small perturbation of solution (20):

$$\begin{aligned}\zeta &= \epsilon \zeta_1 e^{iqx + \omega t}, \\ u &= u_0(z) + \epsilon u_1(z) e^{iqx + \omega t}.\end{aligned}\quad (24)$$

The model equations are to be solved approximately in the presence of this perturbation, and “sufficiently small” then means that we may restrict ourselves to taking it into account only to linear order. Obviously, we may write an ansatz with just a single mode  $\exp(iqx)$ , as any arbitrary perturbation can be expanded in a Fourier series or integral and the linearity of the equations to be examined guarantees that a superposition of solution modes provides a solution as well.

With the wavenumber  $q$  of the mode prescribed, the goal of the analysis is to determine the growth rate  $\omega$ . If the real part of the obtained growth rate is positive, the perturbation will grow, hence the state will be unstable; on the other hand, a negative real part signals stability with respect to perturbations of that wavenumber.

Inserting the ansatz (24) into the diffusion equation (10) we get an ordinary differential equation in  $z$ ,

$$\left[ \frac{d^2}{dz^2} + \frac{2}{\ell} \frac{d}{dz} - \left( q^2 + \frac{\omega}{D} \right) \right] u_1 = 0 \quad (25)$$

which may be solved to obtain the general form of  $u_1$ :

$$u_1(z) = \begin{cases} \alpha_\ell^{(1)} \exp(-\gamma_\ell^{(1)} z) & \text{(liquid)} \\ \alpha_s^{(1)} \exp(-\gamma_s^{(1)} z) & \text{(solid)} \end{cases}. \quad (26)$$

The exponents  $\gamma_\ell^{(1)}$  and  $\gamma_s^{(1)}$  are solutions of quadratic equations. They are uniquely determined by the requirements  $\Re(\gamma_\ell^{(1)}) > 0$  and  $\Re(\gamma_s^{(1)}) < 0$ , ensuring that the boundary conditions (9) are satisfied when  $z$  is sent to  $\pm\infty$ . Providing we define square roots to have non-negative real parts, their values are given by

$$\gamma_\ell^{(1)} = \frac{1}{\ell} + \sqrt{\frac{1}{\ell^2} + q^2 + \frac{\omega}{D}}, \quad (27)$$

$$\gamma_s^{(1)} = \frac{1}{\ell} - \sqrt{\frac{1}{\ell^2} + q^2 + \frac{\omega}{D}}, \quad (28)$$

as long as the – unknown – growth rate  $\omega$  does not acquire a large negative real part. Since the aim of the analysis is to identify regions, where the real part of  $\omega$  changes sign, the forms (28) are the appropriate ones for further investigation.<sup>8</sup>

At this stage, the prefactors  $\alpha_\ell^{(1)}$  and  $\alpha_s^{(1)}$  of the exponentials are as yet undetermined. Equations for them follow from the Gibbs-Thomson relation (7), yielding the temperature boundary condition for both the liquid and solid sides of the interface. Care has to be taken that the evaluation of this condition is done at the interface, which leads to first-order contributions both from  $u_1$  and, via an expansion about  $z = 0$ , from  $u_0$ :

$$\begin{aligned}u(x, \zeta(x, t), t) &= u_0(\zeta) + \epsilon u_1(\zeta) e^{iqx + \omega t} + \mathcal{O}(\epsilon^2) \\ &= u_0(0) + \epsilon \left[ \frac{\partial u_0}{\partial z} \Big|_{z=0} \zeta_1 + u_1(0) \right] e^{iqx + \omega t} + \mathcal{O}(\epsilon^2).\end{aligned}\quad (29)$$

---

<sup>8</sup>In practice, one often introduces the quasistationary approximation at this point already, meaning that  $\omega$  is set equal to zero in the square roots. Then the signs have to be chosen as indicated in all of parameter space.

Using the approximation  $\kappa = -\partial_{xx}\zeta$ , correct to second order in  $\epsilon$ , the resulting values obtained for the amplitudes are [ $d_0 = d(0)$ ]

$$\alpha_\ell^{(1)} = \zeta_1 \left( \frac{2}{\ell} - d_0 q^2 \right), \quad \alpha_s^{(1)} = -d_0 q^2 \zeta_1. \quad (30)$$

Finally, we exploit the continuity equation (6) which is conveniently rewritten as

$$\frac{V + \dot{\zeta}}{D} = \frac{\partial u_\ell}{\partial z} - \frac{\partial u_s}{\partial z} - \frac{\partial \zeta}{\partial x} \left( \frac{\partial u_\ell}{\partial x} - \frac{\partial u_s}{\partial x} \right), \quad (31)$$

where  $u_\ell = u|_\ell$  und  $u_s = u|_s$ , and we have used the decomposition  $n_z = 1/\sqrt{1 + (\partial_x \zeta)^2}$ ,  $n_x = -\partial_x \zeta n_z$  of the interface normal vector. Evaluating the formula at the two-phase interface  $\zeta(x, t)$ , we finally obtain the sought-for *dispersion relation*

$$\frac{\omega}{D} + \left( 2d_0 q^2 - \frac{2}{\ell} \right) \sqrt{\frac{1}{\ell^2} + q^2 + \frac{\omega}{D} + \frac{2}{\ell^2}} = 0. \quad (32)$$

In this implicit form, the equation is not very transparent. Therefore, let us introduce some approximations that are justified in usual experimental situations. First, we assume the quasistationary approximation to hold. This means that we can neglect the time derivative in Eq. (10) or equivalently the  $\omega/D$  term in Eq. (25). As a result, the square root expression in Eq. (32) becomes independent of  $\omega$ . Then (32) already constitutes an explicit equation for the growth rate. Furthermore, experimental conditions are usually such that the approximations  $q\ell \gg 1$  (meaning that the average interface velocity  $V$  is small) and  $d_0 \ell q^2 \ll 1$  (meaning that the capillary length  $d_0$  is small) are well justified. This allows us to replace the square root by  $|q|$  and to neglect summands  $1/\ell \ll |q|$ , which finally leads to the simple form

$$\omega = V|q| (1 - d_0 \ell q^2). \quad (33)$$

This function is positive and linear in  $q$  for small  $q$ , and it becomes negative and cubic for large  $q$ . The maximum of  $\omega(q)$ , the *fastest-growing mode*, is given by  $q_f = (1/3d_0 \ell)^{1/2}$ . Hence, the wavelength  $\rho_{MS}$  corresponding to the fastest-growing mode, the so-called *Mullins-Sekerka length*, behaves as  $(d_0 \ell)^{1/2}$ . Typical capillary lengths are in the Å range, typical diffusion lengths in the cm range. Therefore,  $\rho_{MS}$  is in the  $\mu\text{m}$  range and thus much larger than the capillary length.

It is a reasonable first guess that the length scales of patterns such as a snowflake are comparable with this wavelength. This is based on the idea that with random initial conditions (created by thermal and other noises) all modes will be present with some small amplitude. In the initial phase of growth, described by the linear approximation used here, the fastest-growing mode will then dominate others simply because its amplitude grows to larger values more quickly. It should be noted that this is not what is ordinarily meant by *selection* of a wavelength, because the observation of this wavelength is in fact dependent on the initial condition. Suppose we managed to prepare a system such that a band about the fastest-growing wavelength would be missing in the original state. In such a system, a different wavelength would dominate initial growth. True wavelength selection is a process that leads to a definite length scale independent of initial conditions.

Doing a similar linear stability analysis for the Saffman-Taylor model, we would obtain, without any approximation,

$$\omega = V|q| \left( 1 - \frac{b^2 \gamma}{12 \mu V} q^2 \right), \quad (34)$$

which is essentially the same dispersion relation.

A characteristic feature of both instabilities is that positive growth rates appear for sufficiently small wave numbers, *i.e.*, sufficiently large wavelengths. This kind of instability is called *long-wave instability*. The planar interface is unstable under the smallest driving force, if only the system size is large enough for an unstable mode to show up.<sup>9</sup> Figure 6 displays, on the left panel, a schematic representation of this kind of dispersion relation.

As mentioned above, in the solidification of an alloy, the same formalism applies with the temperature field replaced by a concentration field. The instability is then not driven by the thermal undercooling in the literal sense but by chemical nonequilibrium, leading to the so-called *constitutional undercooling*. A detailed discussion can be found in [22]. Suffice it to say here that by applying a temperature gradient, the average orientation of the interface can be fixed, which leads to suppression of the instability of long-wave modes.

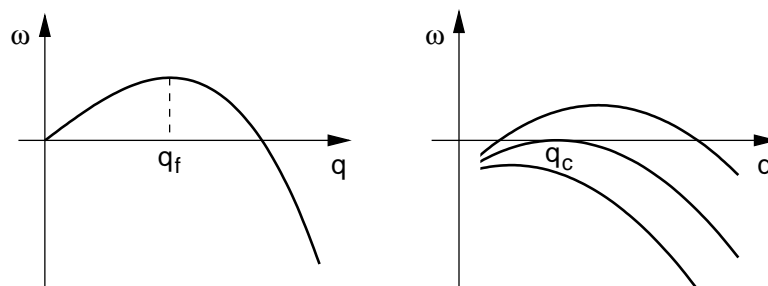


**Fig. 6:** Dispersion relations. Left: Long-wave instability with fastest-growing mode  $q_f$ . Right: Instability with critical wavenumber  $q_c$ .

In fact, the planar interface can be made completely stable by keeping a control parameter that is proportional to the ratio  $V/G$  of the average interface velocity<sup>10</sup>  $V$  and the temperature gradient  $G$  below a critical value. Then the dispersion relation looks like the lowest curve on the right-hand panel of Fig. 6. As  $V/G$  is increased to a critical value, a single mode becomes marginally stable at the *critical wavenumber*  $q_c$ , and with even larger control parameter, a finite band of wavenumbers (and wavelengths) becomes unstable; this is the top curve in Fig. 6, right panel.

### 4.3 Weakly nonlinear analysis

Linear stability analysis can give us an indication, when a basic (usually stationary) state becomes unstable and what are the characteristic wavelengths to be expected from the instability. It cannot tell us anything about the long-time dynamical state of the system after it has gone unstable. For linear stability analysis predicts exponential growth of unstable modes and does not contain any mechanism that would describe saturation effects and the relaxation to a new structure. To obtain such a behaviour, one has to consider nonlinearities.

When the dispersion relation follows the general features of the right-hand side of Fig. 6, it is often possible to derive a useful approximate equation describing the new ordered state, as

<sup>9</sup>At small enough pressure difference, the Saffman-Taylor instability will not develop, unless the Hele-Shaw cell is wide enough.

<sup>10</sup>In this setup,  $V$  can be prescribed by pulling the specimen inside the temperature field towards colder temperatures.

long as the control parameter is only slightly above the instability threshold. Then the dispersion relation can be expanded about its maximum value,  $\omega = \epsilon - a(q - q_c)^2$ ,  $\epsilon$  being a small positive quantity. It is easy to see that the band of unstable wavenumbers has an extension of  $\mathcal{O}(\epsilon^{1/2})$ . This suggests the introduction of slow time and length scales,  $T = \epsilon t$  (because the maximum of  $\omega$  is proportional to  $\epsilon$ ) and  $X = \epsilon^{1/2} x$  (because the band of wave numbers, corresponding to modulations of the wavelength, scales with  $\epsilon^{1/2}$ ). Decomposing the basic field as  $\zeta = A(X, T) \exp(iq_c x)$ , one can derive an *amplitude equation* for the slowly varying quantity  $A(X, T)$ . How to perform such an amplitude expansion systematically is described in some detail in the appendices of [23], a standard reference on pattern formation.

The generic form of the amplitude equation, but not the values of its coefficients, can be gathered from symmetry considerations. It is clear from linear stability analysis that its basic structure must be:  $\partial_t A = \epsilon A + a \partial_{xx} A + \text{higher order terms}$ . Translation of the system by  $\Delta x$  means multiplication with a phase factor  $\exp(iq_c \Delta x)$ , hence translational invariance of the basic equations leads to the requirement that the amplitude equation be invariant with respect to a multiplication of the complex amplitude  $A$  by a phase factor. Since  $A$  will be small near the instability threshold, the dominant higher order terms are those that correspond to small powers of  $A$ . But  $A^2$  is excluded due to translational invariance. The first allowed term is  $|A|^2 A$ . Hence the equation takes the form

$$\partial_T A = A + a \partial_{XX} A - b |A|^2 A. \quad (35)$$

This is the famous *Ginzburg-Landau equation*. If the coefficient  $b$  is positive, this equation gives a correct description of the weakly nonlinear regime, including periodic steady states.<sup>11</sup>

For long-wave instabilities, the Ginzburg-Landau equation is not normally useful. This may even be guessed by straightforward inspection. Neither a snowflake nor a Saffman-Taylor finger can be considered a small-amplitude deviation from a planar interface. We are dealing with the *strongly* nonlinear regime, and this means that generic analytical tools do not lead very far. Rather, analytic approaches must be tailored for the problem at hand, and in the end further insight may be gained only by numerical attacks.

## 5 Nonlinear dynamics – dendrites and fingers

### 5.1 Ivantsov solution

As we saw before, there are no stationary planar solutions, if the nondimensional undercooling  $\Delta < 1$ . However, there do exist other constant-velocity solutions; they were derived in 1947 by Ivantsov [24]. He neglected surface tension effects, an apparently innocent step, given the smallness of the capillary length. In two dimensions, the found solutions are parabolas, given by

$$\zeta = Vt - \frac{1}{2\rho_{\text{tip}}} x^2. \quad (36)$$

Defining the *Péclet number*  $P$  as the ratio of the tip radius and the diffusion length,  $P = \rho_{\text{tip}} V / 2D = \rho_{\text{tip}} / \ell$ , one finds that a condition for the existence of this solution is precisely given by Eq. (23). Unfortunately, this condition is not only necessary but also sufficient, *i.e.*, the undercooling determines the product of  $\rho_{\text{tip}}$  and  $V$  but neither of these quantities is fixed

<sup>11</sup>Otherwise there is no saturation of the amplitude and one would have to go to higher order, but it is not guaranteed that the description will become quantitatively correct at any order, since amplitudes may become too large for a polynomial approximation of nonlinearities to apply.



separately, contrary to the experimental situation where the tip radius and velocity of a dendrite are well-defined once the undercooling is prescribed.

Ivantsov also obtained paraboloids of revolution as three-dimensional solutions, and experiments on dendritic growth from the melt produce structures which may, if only close to their tip, indeed be described by paraboloidal shapes, see Fig. 7.

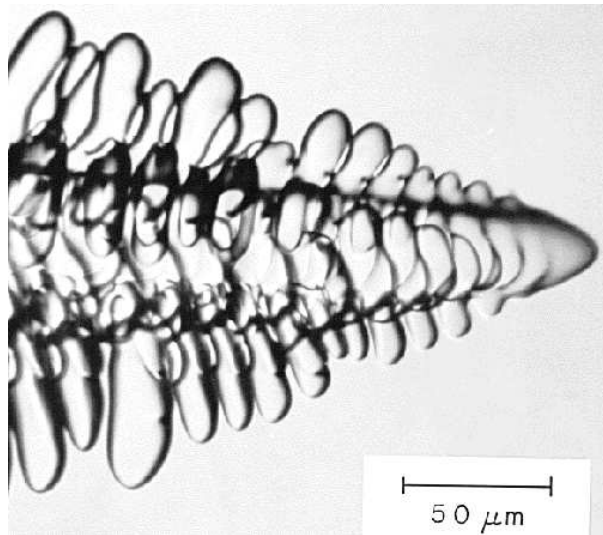


**Fig. 7:** Succinonitrile dendrite growing into undercooled melt. Courtesy M. Glicksman.

But three-dimensional solutions have the same indeterminacy of growth quantities as two-dimensional ones, so we are faced with a *selection problem*: while an Ivantsov paraboloid may qualify as an (approximate) *needle crystal* solution, only to be “decorated” by sidebranches to become a dendrite, we have to explain how a unique solution is selected among the infinitely many possibilities.

The answer to this puzzle must be provided by surface tension. In fact, a linear stability analysis of Ivantsov solutions reveals their unconditional instability due to the absence of surface tension.

## 5.2 Selection theory

Obviously, something dramatic must happen when we take surface tension into account, if this is to exclude an infinity of possible solutions. How can a small perturbation such as the capillary length affect solutions so strongly? This problem is at the heart of the selection problem and it was not solved until 1986 [18, 25, 26]. The key observation is that the curvature term in (7) is a *singular perturbation* [27]. Contrary to regular perturbations, singular ones can change the character of solutions entirely and are thus not negligible in general, even if they are formally small. As an example, consider the simple second-order differential equation  $\epsilon y'' + y = 0$ . For  $\epsilon = 0$ , there is a single solution  $y(x) \equiv 0$ ; for  $\epsilon \neq 0$ , we have a two-parameter family  $y(x) = A \cos(x/\sqrt{\epsilon}) + B \sin(x/\sqrt{\epsilon})$ , definitely not obtainable from the “unperturbed solution” via a perturbation series. The perturbation is singular, because the small term contains the highest derivative. To understand this, it is sufficient to remember that the number of linearly independent solutions of a homogeneous linear differential equation depends on the highest derivative appearing – which is different for  $\epsilon = 0$  and  $\epsilon \neq 0$ .

In order to solve this problem in the case at hand, one proceeds as follows. First, the integral equation (13) is specialized to the stationary case which eliminates the time variable. The remaining equation for  $\zeta(x)$  is considered a problem with certain analyticity properties in all of the complex plane. It then turns out that the contribution of the capillary term is small everywhere except in a small neighbourhood of a pair of singularities. The problem can thus be split in two. Far from the singularities, for the *outer* solution, the capillary term is treated as a small perturbation; close to them, the variation of all the nonsingular terms is negligible which reduces the integral equation to a local *inner* problem (an ordinary complex differential equation). One then has two solutions in different domains of the complex plane that are to describe a globally valid approximation to the true solution. Thus the approximate solutions must be matched to each other in the regions where they overlap, by a technique called *asymptotic matching* [28].

A basic requirement on the solution is that it has vanishing slope at the tip of the needle crystal, otherwise reflection symmetry about  $x = 0$  would imply nonanalytic behaviour. As it turns out, the outer solution has a regular perturbation expansion (in powers of the capillary length) satisfying this requirement at all orders. Matching of the inner solution then demands that even exponentially small terms that ordinarily would be negligible have to be suppressed exactly at this point, because they cannot be argued to be balanced by terms from the regular expansion, which all happen to vanish. Because the inner equation is a second-order nonlinear differential equation, we have two integration constants at our disposal for the matching with the outer solution. Two parameters have to be adjusted to keep the inner solution from diverging exponentially (for large distances from the singularity). But then no degree of freedom is left to make the inner solution vanish at  $x = 0$ , and explicit calculation shows it to be different from zero there. This establishes that no solution to the problem exists. From infinitely many solutions without surface tension, we have moved to *none* with surface tension!

The way out is to realize that surface tension of crystals is anisotropic. Usually, a model expression of the form

$$d(\vartheta) = d_0[1 - \epsilon_m \cos(m\vartheta)] \quad (37)$$

is assumed, with  $m = 4$ . Then we have an additional parameter,  $\epsilon_4$ , that can be tuned to satisfy our third matching condition. As a consequence, we are now back to an infinite but *discrete* family of solutions, of which only one, the solution with the largest velocity, turns out to be linearly stable. Expressed in terms of a nondimensional growth rate  $\sigma$ , often called the stability parameter, the condition for solvability of the integral equation becomes, in the limit of small anisotropy  $\epsilon_4$ ,

$$\sigma \equiv \frac{d_0 V}{2DP^2} = \frac{\epsilon_4^{7/4}}{\lambda_n}, \quad n = 0, 1, 2, \dots, \quad (38)$$

where  $\lambda_n$  is the eigenvalue of a nonlinear problem. In fact, this *solves the selection problem*: taking the smallest eigenvalue  $\lambda_0$ , we have expressions for  $\sigma$  and for  $P$ , which determine both  $V$  and  $\rho_{\text{tip}}$ .

The prediction  $V \sim P^2$  ( $\sim \Delta^4$  for small undercooling) arising from (38) is well confirmed experimentally, even for dendrites with sidebranches. So sidebranches seem to play a rather passive role, hardly affecting the results of *solvability theory*. In fact, WKB techniques developed within it can be used to compute both wavelengths and amplitudes of noise-induced sidebranches [29, 30].

In 2D, the needle crystal solution has a shape that is very close to that of an Ivantsov parabola but with unique velocity and tip radius. In three dimensions, the situation is much more complicated because surface tension anisotropy leads to strong deviations of the needle crystal solution

from the Ivantsov paraboloid. An expansion about the latter is possible only in the vicinity of the dendrite tip, where solvability theory leads to selection of the entire shape including its dependence on the azimuthal angle [31]. The remaining problem of the dendrite tail was solved by Brener [32]. He realized that at the liquid-solid interface the term  $\partial_{zz}u$  of the diffusion equation (10) becomes negligible and the stationary case reduces to a diffusion equation in 2D, *if  $z$  is regarded as time*. This shows immediately that a unique matching of the tail to the tip is possible. Moreover, from analytic and numerical work [33], the solution to the time dependent 2D problem is known. One obtains intermediate asymptotics for the cross-section of the dendrite (parallel to the  $xy$  plane) which is a cross-shaped structure with arm lengths  $\sim |z|^{3/5}$  and arm widths  $\sim |z|^{2/5}$ . It may be added that on the basis of these analytic results, side branching of real dendrites becomes explicable as a consequence of thermal noise.

For Saffman-Taylor fingers, a similar selection problem arises. A continuous family of exact analytic solutions can be given for the hydrodynamic problem (17) – (19), providing the interface tension term  $\gamma\kappa$  in Eq. (19) is neglected [13]. It describes fingers of different widths moving at different velocities. Inclusion of the surface tension term then leads to a solution of the selection problem, this time even with isotropic surface tension [34]. The selected width of the Saffman-Taylor finger is larger than (and for typical experimental conditions close to) half the channel width.

A *needle crystal in a channel* has geometric restrictions similar to those of a Saffman-Taylor finger. It turns out that in this situation the walls provide enough anisotropy to allow stationary finger solutions even with isotropic surface tension – if only  $\Delta > \frac{1}{2}$ . Solvability theory was worked out for this case by Brener, Geilikman and Temkin [35]. They find that as a function of the channel width the selected velocity goes through a maximum where it behaves as  $V \sim (D/d_0)(\Delta - \frac{1}{2})^{7/2}$ . If surface tension is made slightly anisotropic, the solution for the crystal finger approaches that for the free dendrite at large channel widths, its velocity increasing with the width [36]. The Saffman-Taylor finger belongs to a different solution branch: its velocity decreases with increasing channel width.

## 6 Doublons and more complex patterns

As we have seen, the selection problem of dendritic growth (and of viscous fingering) was mathematically reduced to an existence problem first - a continuum of solutions was broken down to a discrete set. Only then could a stability criterion be invoked to choose the single stable state among the discrete solutions. This pretty abstract way of understanding selection seems to result from restricting considerations to stationary solutions of the problem.

To understand things in somewhat more physical terms, it is useful to imagine a *dynamical* state and to ask what would become of an initially parabolic crystal, if surface tension were isotropic. In such a crystal, the tip would be the coldest point of the interface, since the curvature of a needle crystal with parabolic shape (or a shape sufficiently close to parabolic) is maximum at the tip. Therefore, this interface point would experience a smaller driving temperature gradient than the points in its immediate neighbourhood, rendering it vulnerable to a *tip-splitting instability*. As soon as we have surface tension anisotropy, the tip will not be the coldest point anymore, as the prefactor  $d(\vartheta)$  of the curvature is smallest in the growth direction. This has a stabilizing effect on the tip, making steady-state near-parabolic solutions possible.

From this reflection, we infer that isotropic surface tension does *not* necessarily preclude steady-state solutions with shapes that are *far* from parabolic. States such as these have been indeed

discovered by numerical simulations [37, 38], using finite-difference codes and boundary element methods. Consisting of two asymmetric fingers, separated by a channel, they were called *doublons*. A more recent simulation of a structure containing several doublons is shown in Fig. 8.

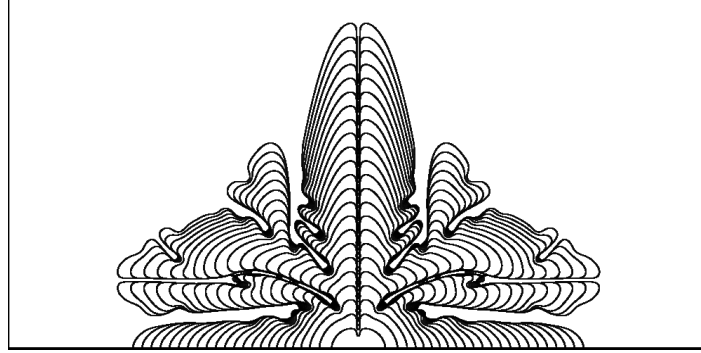


**Fig. 8:** Phase-field simulation of doublons [39]. Different curves correspond to the interface position at equidistant time steps. Parameters:  $\Delta = 0.8$ ,  $\epsilon_4 = 0.01$ .

Doublons escape the tip-splitting instability by having no tip on the symmetry axis. The points of highest curvature are, due to the asymmetry of the single fingers, shifted from their tips to points closer to the inside of the channel separating the fingers. So even with isotropic surface tension the coldest points, tending to lag behind their immediate neighbourhood are safely moved away from the finger tips, allowing stable growth in principle.

The growth mode of doublons is peculiar. Two fingers stabilize each other instead of competing, as one might suspect at first sight, knowing the Mullins-Sekerka instability. In the absence of surface tension anisotropy or with weak anisotropy, a perturbation that puts one of the fingers ahead of the other, will on the one hand tend to assist its growth, because it will move its tip into a region of lower temperature, but on the other hand it will also tend to inhibit growth, because the increased tip curvature lowers the equilibrium temperature due to the Gibbs-Thomson condition. For large enough undercooling, the relative effect of the displacement will be small, as the structure is moving fast anyway, and then the stabilizing surface tension effect should win, which is what seems to happen in the cooperative growth of the fingers of a doublon.

The selection theory for doublons has been worked out [40], albeit at a lower level of rigor than that for dendrites. The resulting expressions for the selected growth velocity and tip radius (of a parabolic envelope) read

$$V \sim \frac{D}{d_0} \Delta^9, \quad \rho_{\text{tip}} \sim d_0 \Delta^{-7}. \quad (39)$$

The existence of a second basic structure besides the dendrite naturally leads to the question which one of the two will prevail under which conditions. Furthermore, one may consider the question of the long-time dynamics of structures. The side branches of a dendrite may evolve into new dendrites, giving rise to a space-filling dendritic structure.

More generally, a growing circular nucleus will, due to the Mullins-Sekerka instability, develop protrusions and troughs, once it exceeds a certain size. Initially, the dimensions of these features will be on the order of the Mullins-Sekerka length  $\rho_{MS}$ . In the course of time, they will develop into fingers which grow larger and wider. If the undercooling is low and/or the anisotropy high, they will evolve into dendrites producing side branches. If the undercooling is large and/or

the anisotropy low, they will undergo repeated tip splitting processes. But as soon as a deep channel has formed between two fingers, they can survive as a doublon. The ensuing pattern has been termed (compact) seaweed structure [41, 42]. An example for an experimental seaweed structure, obtained in a liquid-crystal experiment is shown in Fig. 9.

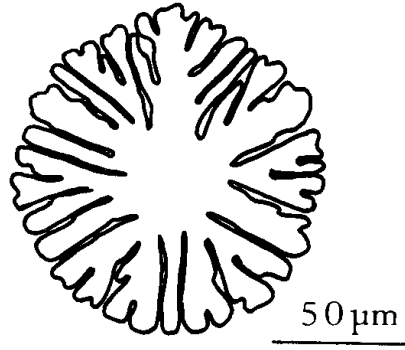


**Fig. 9:** Growth of the columnar hexagonal crystal hexaoctyloxytriphenylene. Phase boundary redrawn after a photograph (courtesy of P. Oswald) [43].

One may then draw a kinetic phase diagram or *morphology diagram* indicating which structures are to be expected in which part of parameter space. Here, we have only two relevant parameters, the surface tension anisotropy  $\epsilon (= \epsilon_4)$  and the undercooling  $\Delta$ , so the diagram can be conveniently represented in two dimensions. The decision between different morphologies coexisting in a region of parameter space is made by consideration of their velocity: the faster one wins.

The current theoretical status is summarized by Fig. 10. There are four kinds of morphologies, of which we have already discussed the *compact dendritic structure* (CD) and the *compact seaweed* (CS).

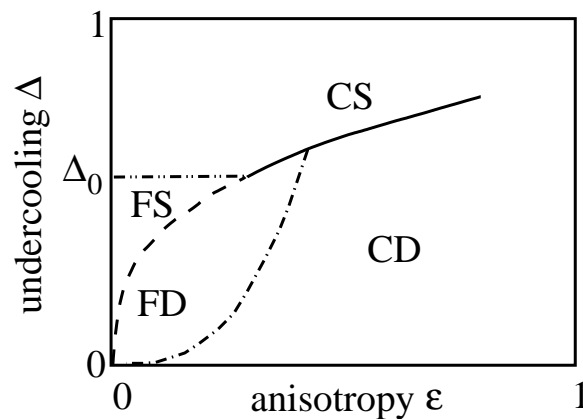


**Fig. 10:** Morphology diagram for diffusion-limited growth, displaying the regions of predominance of compact dendrites (CD), compact seaweed (CS), fractal dendrites (FD), and fractal seaweed (FS).

The dendritic structure in principle exists in the whole parameter plane indicated. But whenever

doublons exist, and they do so below a certain value of the anisotropy for given undercooling, they seem to be faster than dendrites, so the seaweed structure, the building blocks of which are doublons, should dominate. Behind all of this, there is the hypothesis, rather well confirmed in experiments with dendrites, that structures grow as fast as their basic building blocks. At very low anisotropies and undercoolings, thermal noise affects the structures strongly and destroys their compactness, rendering them *fractal* in a certain range of length scales.

Therefore, we have a *fractal dendritic* (FD) and a *fractal seaweed* (FS) structure, with different scaling laws for characteristic length scales and velocities, deduced in Ref. [42]. In the derivation, another velocity selection mechanism is invoked, going back to Uwaha and Saito [44]. This is selection via the fractal dimension. Unfortunately, space limitations do not permit a discussion of this interesting mechanism here. An impression what a fractal seaweed looks like can be gathered from Fig. 3.

The transition between the FD and FS structures is just a crossover, whereas that between the CD and CS patterns has the characteristics of a first-order phase transition.

## 7 Summary and outlook

Theoretical knowledge about diffusion-limited growth of a nucleus of one phase in another in two dimensions is summarized in the morphology diagram given in Fig. 10. The basic ideas entering this description are selection theory and scaling arguments. Three selection mechanisms are operative, selection by anisotropy of surface tension (leading to dendrites), selection by surface tension alone (leading to doublons) and selection by fractal dimension in combination with noise. Of the diverse selection theories the one elaborated to the deepest level of detail is still the solvability theory for dendritic growth; it is also the only one, where results have been fully extended to three dimensions.<sup>12</sup>

In 3D, Doublons should become triplons, *i.e.*, three-finger structures, but there is no analytic theory available for these yet. Neither is there a morphology diagram analogous to Fig. 10 (with quantitative relationships) in the three-dimensional case.

Another extension besides going to three dimensions would be to include further relevant transport mechanisms such as convection. If convection is added, we may expect the transition lines between dendritic and seaweed structures to change with flow conditions. In fact, the diagram should become three-dimensional, with a parameter describing flow strength added.

Selection theory for dendritic growth in the presence of flow is rudimentary, to say the least. There is a theory, based on the solvability approach, by Bouissou and Pelcé [45] which however seems to be contradicted by experiments [46].

On the other hand, there are already a number of simulations of dendritic growth including convection. A promising approach seems to be to combine the phase-field method (lecture B. Nestler) with a lattice-Boltzmann algorithm (lecture M. Ripoll). Fig. 11 shows a seaweed structure simulated this way [39]. A shear flow moving cold fluid into the system from the left has been imposed, with undercooling and surface tension anisotropy the same as in Fig. 8. The upward-growing doublon bends into the incoming flow. Dendrites do not do quite the same thing [39].

These numerical methods may then be used to measure the selected values of growth velocity, tip radius, and hence the stability parameter  $\sigma$ , in order to guide selection theory. An interesting

<sup>12</sup>For Saffman-Taylor fingers, the three-dimensional version of the problem refers to an entirely different physical situation. In 3D, Darcy's law holds only in a porous medium.

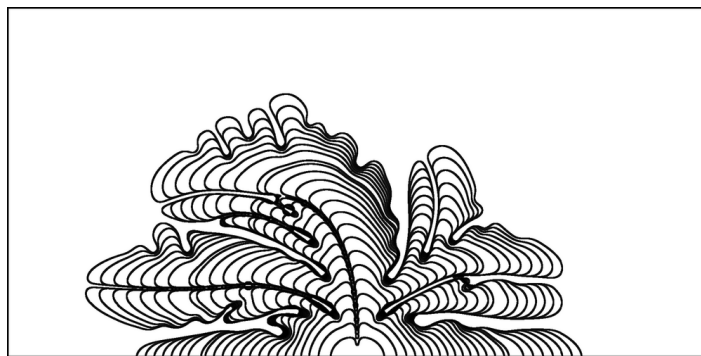


**Fig. 11:** *Doublon exposed to shear flow.  $\Delta = 0.8$ ,  $\epsilon_4 = 0.01$ , Prandtl number  $Pr = \nu/D = 1.78$  ( $\nu = \mu/\rho$ ). Fluid velocity imposed at the top of the box in the  $x$  direction:  $U_0 = 0.0987D/d_0$ .*

result, obtained from the simulation of a dendrite in a flow imposed antiparallel to its growth direction, is shown in Fig. 12: different data points correspond to different values of undercooling, Prandtl number and imposed flow velocity at fixed surface tension anisotropy. They all fall on the same curve, displaying the measured stability parameter  $\sigma$  (defined in Eq. (38)) versus the Péclet number. This shows that no matter how we choose, say, the combination of undercooling and imposed flow velocity to obtain a certain value for the Péclet number, we should get the same growth velocity and tip radius of the dendrite. A selection theory including convection should be able to reproduce this feature.

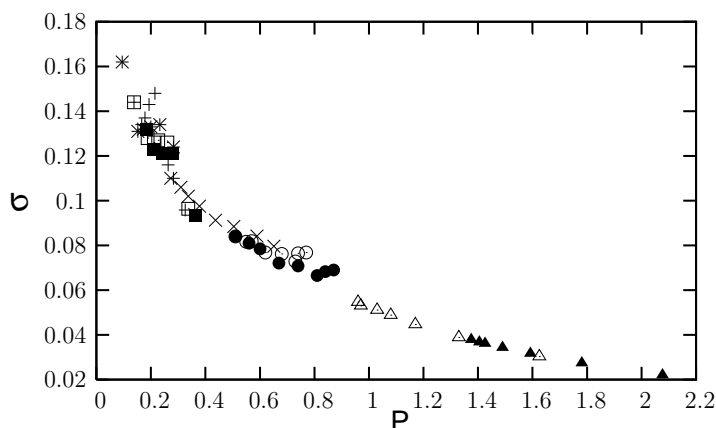


**Fig. 12:** *Selection for dendrites in flow. The anisotropy is  $\epsilon_4 = 0.05$  for all points, the undercooling varies between  $\Delta = 0.45$  and  $\Delta = 0.80$ , the Prandtl number between  $Pr = 0.83$  and  $Pr = 5.00$ . Data points with the same symbol correspond to fixed  $\Delta$ ,  $Pr$ , but varying imposed flow velocity.*

## References

- [1] *Oscillations and Traveling Waves in Chemical Systems*, eds. R.J. Field, M. Burger (Wiley, New York, 1985).

- [2] A. Turing, Phil. Trans. Roy. Soc. London, Ser. B **237**, 37 (1952)
- [3] P. de Kepper, V. Castets, E. Dulos, J. Boissonade, Physica D **49**, 161 (1991)
- [4] G.I. Sivashinsky, Acta Astronautica **4**, 1177 (1977)
- [5] T. Ackemann, Yu. A. Logvin, A. Heuer, W. Lange, Phys. Rev. Lett. **75**, 3450 (1995)
- [6] Yu.A. Astrov, E. Ammelt, S. Teperick, H.-G. Purwins, Phys. Lett. A **211**, 184-190 (1996)
- [7] F.-J. Niedernostheide, M. Kreimer, H.-J. Schulze, H.-G. Purwins, Phys. Lett. A **180**, 113 (1993)
- [8] R. Graham, H. Haken, Z. Physik **237**, 31 (1970)
- [9] K. Brattkus and C. Misbah, Phys. Rev. Lett. **64**, 1935 (1990)
- [10] C. Darwin, *On the Origin of Species by Means of Natural Selection or the Preservation of Favored Races in the Struggle of Life* (Murray, London, 1859).
- [11] T. Kobayashi and T. Kuroda, in *Morphology of Crystals, Part B*, ed. I. Sunagawa (Terra Scientific Publishing, Tokyo, 1987), p. 645
- [12] W.W. Mullins and R. F. Sekerka, J. Appl. Phys. **34**, 323 (1963), J. Appl. Phys. **35**, 444 (1964)
- [13] P.G. Saffman, G. Taylor, Proc. Roy. Soc. A **245**, 312 (1958)
- [14] Y. Saito, G. Goldbeck-Wood, H. Müller-Krumbhaar, Phys. Rev. A **38**, 2148 (1988)
- [15] M. Glicksman, R.J. Schaefer, J.D. Ayers, Metall. Trans. A **7**, 1747 (1976)
- [16] M.E. Glicksman, S.P. Marsh, *The Dendrite*, in *Handbook of Crystal Growth Ib, Transport and Stability*, ed. D.T.J. Hurle (Elsevier, Amsterdam, 1993)
- [17] H. Müller-Krumbhaar, T. Burkhardt, D. Kroll, J. Cryst. Growth **38**, 13 (1977)
- [18] B. Caroli, C. Caroli, B. Roulet, J. Langer, Phys. Rev. A **33**, 442 (1986)
- [19] K. Kassner, *Pattern formation in diffusion-limited crystal growth* (World Scientific, Singapore, 1996)
- [20] *Handbook of Mathematical Functions*, eds. M. Abramowitz, I. Stegun (Dover, New York, 1972)
- [21] J.S. Langer, in *Chance and Matter*, eds. J. Souletie, J. Vannimenus, R. Stora (Elsevier, Amsterdam, 1987), p. 629
- [22] K. Kassner, *Musterbildung im Kristallwachstum*, in *Komplexe Systeme zwischen Atom und Festkörper* (25. IFF-Ferienkurs, FZ Jülich, 1994)
- [23] M.C. Cross, P.C. Hohenberg, Rev. Mod. Phys. **65**, 851 (1993)



- [24] G.P. Ivantsov, Dokl. Akad. Nauk. SSSR **58**, 567 (1947); an English translation can be found in [47], p. 243
- [25] M. Ben Amar, Y. Pomeau, Europhys. Lett. **2**, 307 (1986)
- [26] A. Barbieri, D.C. Hong, J.S. Langer, Phys. Rev. A **35**, 1802 (1987)
- [27] E. Ben-Jacob, N. Goldenfeld, J.S. Langer, G. Schön, Phys. Rev. Lett. **51**, 1930 (1983); Phys. Rev. A **29**, 330 (1984)
- [28] C.M. Bender, S.A. Orszag, *Advanced Mathematical Methods for Scientists and Engineers* (McGraw-Hill, New York, 1978)
- [29] M.N. Barber, A. Barbieri, J.S. Langer, Phys. Rev. A **36**, 3340 (1987)
- [30] J.S. Langer, Phys. Rev. A **36**, 3350 (1987)
- [31] M. Ben Amar, E. Brener, Phys. Rev. Lett. **71**, 589 (1993).
- [32] E. Brener, Phys. Rev. Lett. **71**, 3653 (1993)
- [33] R. Almgren, W.-S. Dai, V. Hakim, Phys. Rev. Lett. **71**, 3461 (1993)
- [34] R. Combescot, T. Dombre, V. Hakim, Y. Pomeau, A. Pumir, Phys. Rev. Lett. **56**, 2036 (1986); Phys. Rev. A **37**, 1270 (1988)
- [35] E.A. Brener, M.B. Geřlikman, D. E. Temkin, Sov. Phys. JETP **67**, 1002 (1988)
- [36] E.A. Brener, V.I. Mel'nikov, Adv. Phys. **40**, 53 (1991)
- [37] T. Ihle, H. Müller-Krumbhaar, Phys. Rev. E **49**, 2972 (1994)
- [38] E. Brener, Y. Saito, H. Müller-Krumbhaar, D. Temkin, Pis'ma Zh. Ėksp. Teor. Fiz. **61**, 285 (1995) [JETP Lett. **61** 185 (1995)]
- [39] D. Medvedev, K. Kassner, Phys. Rev. E **72**, 056703 (2005)
- [40] M. Ben Amar, E. Brener, Phys. Rev. Lett. **75**, 561 (1995)
- [41] E. Brener, H. Müller-Krumbhaar, D. Temkin, Europhys. Lett. **17**, 535 (1992); E. Brener, K. Kassner, H. Müller-Krumbhaar, D. Temkin, Int. J. Mod. Phys. C **3**, 825 (1992)
- [42] E. Brener, H. Müller-Krumbhaar, D. Temkin, Phys. Rev. E **54**, 2714 (1996)
- [43] P. Oswald, J. Malthête, P. Pelcé, J. Phys. France **50**, 2121 (1989)
- [44] M. Uwaha, Y. Saito, J. Phys. Soc. Jap. **57**, L3285 (1988), Phys. Rev. A **40**, 4716 (1989)
- [45] P. Bouissou, P. Pelcé, Phys. Rev. A **40**, 6673 (1989)
- [46] Y.-W. Lee, R. Ananth, W. Gill, J. Cryst. Growth **132**, 226 (1993)
- [47] *Dynamics of Curved Fronts*, ed. P. Pelcé (Academic Press, Boston, 1988)